# STANDARDIZATION OF H$\alpha$ PHOTOMETRY

by

Laura Adams

A senior thesis submitted to the faculty of

Brigham Young University

in partial fulfillment of the requirements for the degree of

Bachelor of Science

Department of Physics and Astronomy

Brigham Young University

April 2009

Copyright © 2009 Laura Adams

All Rights Reserved

BRIGHAM YOUNG UNIVERSITY

DEPARTMENT APPROVAL

of a senior thesis submitted by

Laura Adams

This thesis has been reviewed by the research advisor, research coordinator, and department chair and has been found to be satisfactory.

| | |
|---|---|
| Date | Michael D. Joner, Advisor |
| Date | Eric Hintz, Research Coordinator |
| Date | Ross Spencer, Department Chair |

ABSTRACT

# STANDARDIZATION OF H$\alpha$ PHOTOMETRY

Laura Adams

Department of Physics and Astronomy

Senior Thesis

Balmer series line strength is known to depend on photospheric stellar temperature. In the past astronomers relied on the H$\beta$ line to determine the temperature of spectral type B, A, and F stars. The development of detectors that are more sensitive to red wavelengths now makes it easier to observe the H$\alpha$ line. This thesis presents a list of the H$\alpha$ values for several standard stars scattered throughout the sky and easily viewed from the northern hemisphere. Stars from the Pleiades, Hyades, Coma, and NGC 752 star clusters are included as well. This color index may be used to determine stellar temperature for spectral type B, A, F, G, and K stars. The observation method is independent of instrumentation. Data were obtained at the West Mountain Observatory of Brigham Young University.

# ACKNOWLEDGMENTS

I would like to thank Professor Joner for including me in this project and for the countless hours he spent guiding me through it.

# Contents

**Acknowledgments** **v**

**Table of Contents** **vi**

**List of Tables** **viii**

**List of Figures** **ix**

**1 Introduction** **1**

1.1 Stellar Temperature . . . . . 1

1.1.1 Motivation . . . . . 1

1.1.2 Methods of Determination . . . . . 2

1.2 Dual Wavelength Color Index . . . . . 4

1.2.1 Various Systems . . . . . 4

1.2.2 Challenges of Measuring Color . . . . . 6

1.3 Single Wavelength Color Index . . . . . 7

1.3.1 Balmer Series Line . . . . . 7

1.3.2 Method . . . . . 8

1.3.3 Determining Temperature . . . . . 8

1.3.4 Advantage over dual wavelength . . . . . 10

1.4 Advantage of H$\alpha$ over H$\beta$ . . . . . 11

**2 Observations** **13**

2.1 Targets . . . . . 13

2.2 Data Collection . . . . . 15

2.3 Equipment . . . . . 15

2.3.1 West Mountain Observatory . . . . . 15

2.3.2 Telescopes and filters . . . . . 16

2.3.3 Charge-Coupled Devices . . . . . 17

**3 Data Reduction** **19**

3.1 Calibration frames . . . . . 19

3.1.1 Bias Frames . . . . . 19

3.1.2 Dark Frames . . . . . 19

3.1.3 Flat Frames . . . . . 20

3.2 Aperture Photometry . . . . . 20

**4 Data analysis and results** **22**

4.1 Results . . . . . 22

4.2 Conclusion . . . . . 29

**Bibliography** **30**

**References** **30**

**A Stellar Data** **32**

**B Balmer Discontinuity** **35**

**C Charge Coupled Devices** **37**

**Index** **39**

## List of Tables

1.1 Strömgren filters . . . . . 6
4.1 Results . . . . . 22
A.1 Target star data . . . . . 32

## List of Figures


1.1 Spectral line temperature dependence . . . . . 3
1.2 Stellar radiation curves . . . . . 5
1.3 Hydrogen line temperature dependence . . . . . 9
2.1 NGC 752 . . . . . 14
2.2 West Mountain Observatory. . . . . 16
2.3 The 0.31 meter telescope . . . . . 17
3.1 Aperture and annulus . . . . . 21
4.1 Visible magnitudes versus H$\alpha$ graphs . . . . . 26
4.2 B-V versus H$\alpha$ graph . . . . . 28

# Chapter 1

# Introduction

## 1.1 Stellar Temperature

### 1.1.1 Motivation

Developing models of stellar evolution has been a difficult task. Stars similar in mass to the sun live for about $10^{10}$ years, but researchers have been collecting data on stars for only one hundred years. That is one one-hundred millionth of a stellar life cycle (Freedman 2005). Determining the life cycle of a star with such little observation is similar to trying to understand the human life cycle by observing humans for about twenty-five seconds. Things are further complicated by the opacity of stars which prevents astronomers from seeing the processes that go on inside a star (Freedman 2005). Fortunately, there are a few things that make this daunting task possible.

Although we could never watch one star live out its entire life, we can look at several stars in various stages of their life cycle. The Milky Way Galaxy alone has billions of stars that vary in both age and mass(Freedman 2005). Stars that are roughly the same mass will evolve similarly. By looking at how similar stars look at different ages, astronomers can get an idea of how stars change over specific periods of time.

This understanding has been solidified by mathematical models that were developed after careful study of our own star, the sun. For example, astronomers have used the vibrations of the sun's surface to determine the sun's density and put constraints on stellar models. Astronomers determined that the sun must be fueled by nuclear reactions because it has to be at least as old as the earth and no chemical reaction could sustain it for that long (Freedman 2005). Using this knowledge and

principles such as the ideal gas law, hydrostatic equilibrium, and gravitational sources of energy, astronomers have developed models of stellar evolution. These models are dependent on various stellar properties, one of which is the star's temperature (Zeilik and Gregory 1998).

In this thesis we present a method of accurately determining stellar temperature (by temperature we mean the temperature of the star's photosphere). While other methods do exist, they require corrections that our method does not require. Erroneous corrections lead to inexact temperature measurements. We will discuss the other methods and explain why our method is more favorable.

### 1.1.2 Methods of Determination

One way to determine stellar temperature is to examine the spectrum of a star. Some of the light that comes from the hot stellar interior is absorbed as it passes through the cool layers of the star's atmosphere. The resulting spectrum has dark lines which mark photons that were absorbed in the atmosphere.

The absorption lines that appear depend on both the star's composition and temperature. All stars contain a significant amount of helium, but not all stellar spectra contain ionized helium lines. Only stars whose temperature is at least 30,000 K produce enough energy to excite the tightly bound electrons and produce absorption lines. Therefore, if ionized helium lines appear we know that star's temperature is above 30,000 K. In contrast, only cool stars contain molecules. The bonds that hold molecules together are much weaker than those that hold an electron to an atom. Above 3,000 K molecular bonds break and molecules no longer form within the star. Figure 1.1 shows the temperature dependence of other spectral features (Freedman 2005). The strength of the hydrogen line will be discussed in Section 1.3.3.

Astronomers can use a star's spectrum to determine the star's temperature to a high degree of accuracy, but this method has its limitations. The main problem is that the process is lengthy. Each spectral feature must be analyzed carefully to determine which transition created that line.

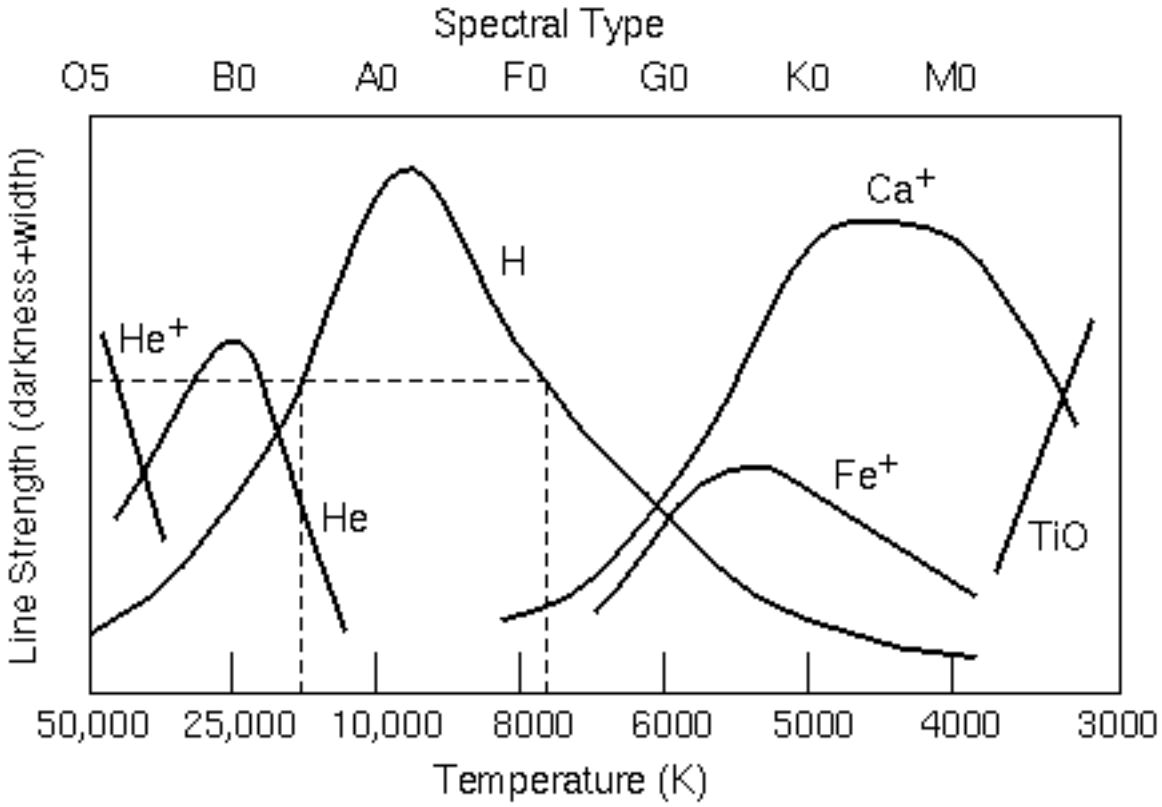


**Figure 1.1:** Temperature dependence of various spectral lines including the hydrogen line. Molecular lines are found in cool stars while ionized helium lines are found in stars hotter than 30,000 K. Image was taken from http:
www.astronomynotes.com/starprop/linestr.gif.

Alternatively,the star's color can be measured, but how is color quantified? If two stars are blue, which star is bluer and by how much? Astronomers quantify color using a star's color index—the difference in a star's magnitude as measured through two or more filters. Because color depends on magnitude difference, this method does not depend on the distance to the star (Zeilik and Gregory 1998). Various types of color indices will be discussed in the next section.

## 1.2 Dual Wavelength Color Index

### 1.2.1 Various Systems

The first type of color index is the dual wavelength index. In this system two filters are centered on two different wavelengths. Taking the difference between the magnitudes measured through each filter yields the color index. The long wavelength is always subtracted from the short wavelength.

The dual wavelength index exploits the fact that stellar radiation is temperature dependent. Figure 1.2 shows the intensity curves for stars of various temperatures. The 12,000 K star radiates blue wavelengths more intensely than red, so the magnitude of the blue filter will be lower. As a result, this star will have a negative color index. On the other hand, the 3000 K star radiates more intensity towards the red end of the spectrum, giving this star a positive color index. By measuring how positive or negative a star's color index is, one can determine how red or blue that star is. This system is dependent on instrumentation, so the index has been calibrated so that a 10,000 K star has a 0.0 index. Stars that are cooler than this will have a positive color index, and stars hotter than 10,000 K will have a negative color index.

For reasons that will be discussed later, stellar temperature is not uniquely determined by just one color index (Zeilik and Gregory 1998). At least three colors are needed to accurately determine the star's temperature. Several systems have

been developed. The UBV system involves three filters whose bandwidth is approximately 1000 Å. These filters are centered at 3650 Å, 4400 Å, and 5500 Å respectively (Zeilik and Gregory 1998).

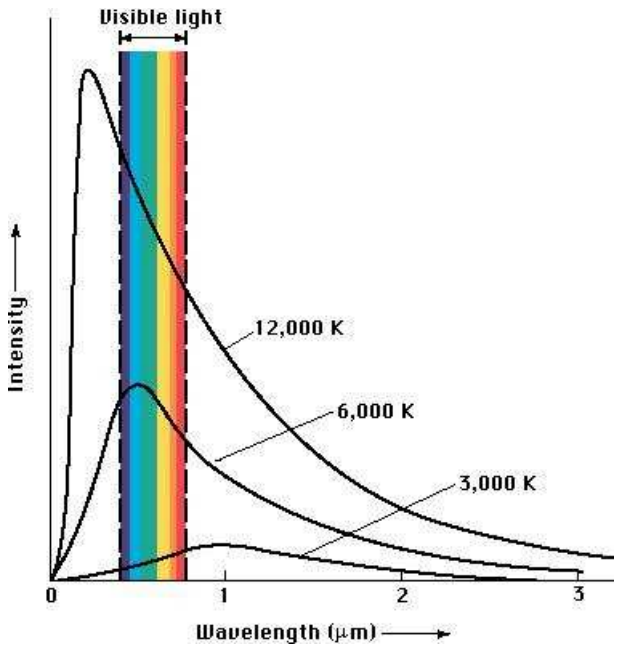


**Figure 1.2:** Radiation curves for various stellar temperatures. Hotter stars emit their peak intensities at blue to ultraviolet wavelengths. Cool stars emit their peak intensities at red to infrared wavelengths. Image was taken from www.astro.ncu.edu.tw/~wchen/Courses/Ast101/blackbody_curves.jpg.

Another commonly used system is the Strömgren *uvby* system (Olsen 1993), which includes four filters. The filters and their properties are shown in Table 1.1. This system was created to overcome inaccuracies in the UBV system due to the Balmer jump. (See Appendix B for more information on the Balmer jump). The $y$ filter is centered on the same wavelength as the V filter in the UBV system. A measurement of visual magnitude through the $y$ filter is equivalent to measure visual magnitude through the V filter. The $b-y$ color index can be used to determine temperature just as the B−V color index.

| Filter | Central Wavelength (Angstroms) | Full Width at Half Transmission (Angstroms) |
|---|---|---|
| $y$ | 5500 | 200 |
| $b$ | 4700 | 100 |
| $v$ | 4100 | 200 |
| $u$ | 3500 | 400 |

**Table 1.1:** Strömgren *ubvy* Filters

### 1.2.2 Challenges of Measuring Color

While a star's color is intrinsic, the color we measure may not be the same as this intrinsic color. As starlight travels through space it encounters gas and dust which scatters the light. As a result, the star appears dimmer than it actually is—up to two magnitudes per every thousand parsecs (Budding 1993). Additionally, not all light is scattered equally. Blue light is scattered more than red light, causing the star to appear redder than it actually is (Freedman 2005). This effect is known as interstellar reddening. The difference between the actual color index and the reddened color index we observe is called the color excess (Zeilik and Gregory 1998).

Using a three–color index makes it possible to determine the effects of reddening. However, this process is difficult. The total interstellar reddening is dependent on both the wavelength observed and how much interstellar material the light had to travel through (Zeilik and Gregory 1998). Any measurement errors lead to an incorrect color index.

In addition to making corrections for interstellar scattering, astronomers also have to compensate for atmospheric scattering. The degree of atmospheric scattering depends on several factors including cloud cover, the amount of dust in the atmosphere, and the height of the star relative to the horizon, to name a few. To avoid extinction due to clouds and dust, the stars are observed only on photometric nights—nights with no cloud cover and minimal pollution. Compensating for the star's location requires more work. Near the zenith there is approximately one atmosphere of extinction, while at the horizon there is a good deal of extinction as the starlight must pass through more atmosphere. By measuring the magnitude of a standard star at various zenith angles, one can determine the level of extinction per unit sec z, also called an airmass. This can then be applied to other stars observed during a night (Zeilik and Gregory 1998).

## 1.3 Single Wavelength Color Index

### 1.3.1 Balmer Series Line

By the early 20th century, a lot of work had already been done on atomic spectra, but the model was incomplete. Physicists had discovered that atoms emit a unique spectrum; that the absorption lines of an atom correspond to its emission lines; and the existence of helium on the sun prior to its discovery on earth (Fowler 2008). Despite all this work, they still did not have a satisfactory explanation of how those lines form. The most promising explanation came in 1913 when Niels Bohr proposed his model of the hydrogen atom.

Bohr postulated that electrons orbit the nucleus in discrete, stable orbits. Each orbit has a certain energy associated with it. When an electron is excited from a lower energy to a higher energy level, it absorbs a photon with an energy equal to the difference of energy levels. This creates absorption lines. Emission lines are created when an electron moves to a lower energy level and releases the extra energy as a photon (Zeilik and Gregory 1998).

Several series of hydrogen spectral lines have been discovered. The first was the Balmer series. These transitions correspond to electrons in the second energy level, n=2, jumping to a higher energy level. The jump from n=2 to n=3 is known as the H$\alpha$ line, the line from the n=2 to n=4 transition is the H$\beta$ line, and so forth. Other series include the Paschen, Brackett, and Pfund series corresponding to excitation from the n=3, n=4, and n=5 energy levels respectively (Zeilik and Gregory 1998). Balmer lines, especially the H$\beta$ line, have been used in single wavelength color indices.

### 1.3.2 Method

The single wavelength index involves two filters which measure the strength of a spectral feature. One of the filters has a narrow bandpass while the other has a wide bandpass (Budding 1993). The narrow filter measures the amount of light coming through the line. A small amount of light coming through means much of that light was absorbed in the star's atmosphere. The wide filter measures the surrounding continuum. Taking the difference between each filter's magnitude then gives an N$-$W color index. The larger the index, the stronger the line is.

### 1.3.3 Determining Temperature

For our purposes, we need to calibrate the N$-$W color index to a temperature scale. As mentioned previously, spectral line strength depends on the star's temperature. Since we will be dealing with hydrogen lines, it is important to understand how they are temperature dependent. A graphical description of this may be seen in Figure 1.3.

Cool stars have weak hydrogen lines; this is because exciting electrons to higher energy levels requires a certain amount of energy. The least energetic line, the H$\alpha$ line, requires the energy carried by a red photon. Cool stars radiate mostly in the infrared, so they do not produce enough red photons to excite a significant number of electrons.

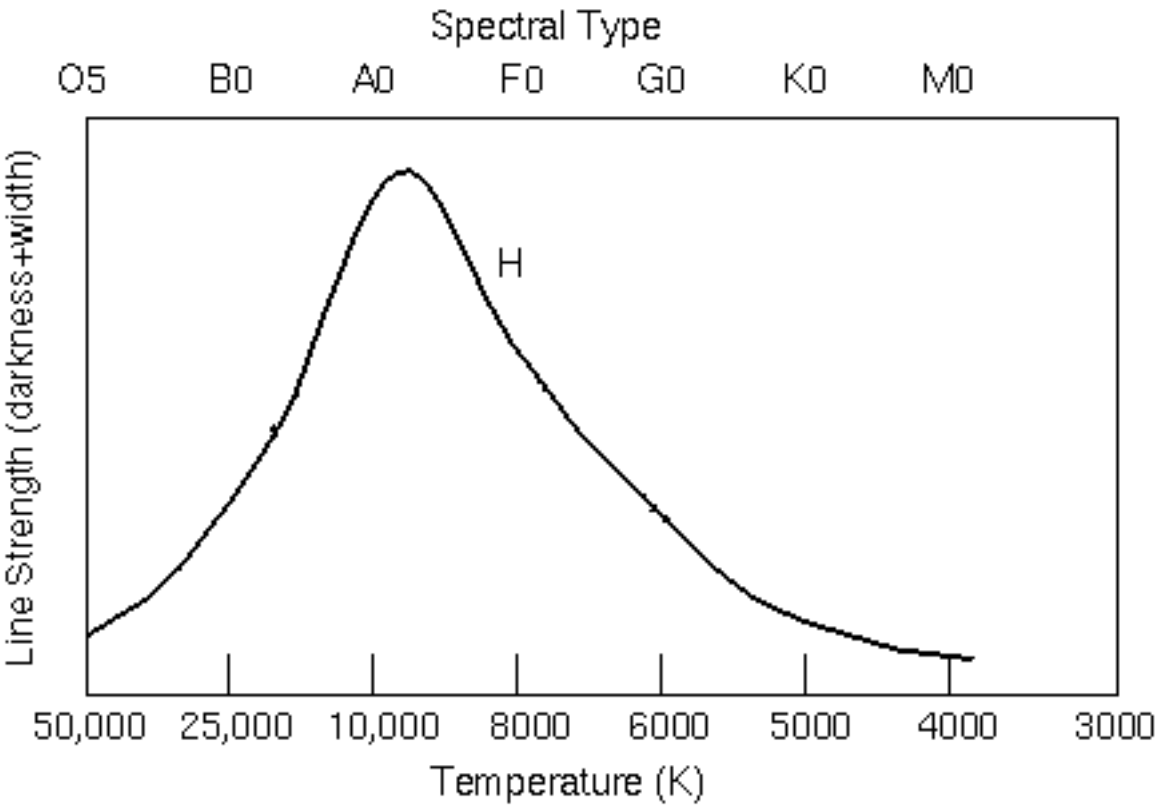


**Figure 1.3:** Temperature dependence of the hydrogen line. Cool stars lack sufficient energy to excite the electrons. Type A stars have the strongest H$\alpha$ lines because they are hot enough to excite several electrons, but not hot enough to ionize hydrogen. Stars hotter than this begin to ionize hydrogen, so they have weaker lines. This figure was taken from http://www.astronomynotes.com/starprop/linestr.gif and curves of other spectral features were removed.

Hotter stars produce a greater quantity of red photons. Eventually, the hydrogen lines become strongest in A type stars. After this, the line again decreases. This decrease is not due to a lack of red photons. Although hot stars emit their peak intensities at the blue end of the spectrum, they still produce more red photons than cooler stars. The decline occurs because the stars are so hot that more and more hydrogen is ionized. Without electrons in the excited states, no transition occurs and the line becomes weak in hot O and B type stars.

### 1.3.4 Advantage over dual wavelength

Single wavelength color indices are preferable to dual wavelength indices because they are free from both atmospheric and interstellar extinction. As stated earlier, scattering is dependent on wavelength. In dual wavelength color indices the light that comes through each filter is scattered differently. In single wavelength indices both filters are centered on the same wavelength so they are equally affected by scattering. As a result, no corrections for reddening need to be made and there are fewer ambiguities (Crawford and Mander 1966).

The freedom from reddening speeds up the process of finding a star's color index. In the dual wavelength color index at least three colors are needed in order to account for reddening effects (Zeilik and Gregory 1998). Two filters are sufficient for the single wavelength index and thus fewer exposures of the star can be taken.

Finally, N−W work can be done in conditions that would be too poor for dual wavelength color indices (Crawford and Mander 1966). Cloud coverage causes variable atmospheric extinction, making it impossible to do dual wavelength photometry even on nights with a few scattered clouds. Because the N and W filters are equally affected, photometry can be done as long as the atmospheric conditions remain roughly constant during both the N and W exposures (Crawford and Mander 1966).

## 1.4 Advantage of H$\alpha$ over H$\beta$

The H$\beta$ index has been the most commonly used single wavelength color index. At the time it was developed, photomultipliers were the detector of choice. This instrument has a higher quantum efficiency (QE) at blue wavelengths than at red wavelengths. Higher quantum efficiency means that a higher percentage of the incident photons will be detected. As this is where the H$\beta$ line is located, it made sense to observe that line. The detector did not have enough sensitivity at red wavelengths to observe the H$\alpha$ line in a significant number of stars (Dachs and Schmidt-Kaler 1975). In fact, early photomultipliers had essentially no response at wavelengths greater than 650 nm.

The charge coupled device (CCD) is now the most commonly used detector in research astronomy. This makes it both possible and advantageous to observe the the H$\alpha$ line. A CCD's peak QE is at red wavelengths, right where the H$\alpha$ line is. The exposures can then be shorter and still yield high quality data, allowing for more observations in a single night.

Several properties of the H$\alpha$ line make it a better choice than the H$\beta$ line. First, the H$\alpha$ line can be measured in a wider temperature range than the H$\beta$ line. As seen in Figure 1.2, cool stars emit their peak intensities at red wavelengths, so we want to observe a spectral line that is located there. Although hot stars emit more light at blue wavelengths, they still emit a lot of red light so we can easily measure their H$\alpha$ line as well.

Another advantage is that the H$\alpha$ line is intrinsically stronger than the H$\beta$ line, especially in late type stars. To produce an H$\beta$ line, a star must be hot enough to excite a significant number of electrons into the n=3 energy level. Cool stars do not have enough energy to do this, but they do have enough energy to excite electrons into the n=2 energy level. As a result, they have a stronger H$\alpha$ line.

Finally, the H$\alpha$ line has fewer surrounding spectral features. The H$\beta$ line lies near the Balmer discontinuity. There are several other absorption lines in this area

that may interfere with measurements of the H$\beta$ line, especially those taken through the wide filter which measures a wider range of wavelengths.

# Chapter 2

# Observations

## 2.1 Targets

Our color index catalogue contains a total of 116 stars. Only 30 of these stars are field standards; the rest are found in star clusters. Eighteen of the stars are in the Coma cluster, 29 are in the Pleiades, 10 are in the Hyades, and 29 of them are found in NGC 752. The NGC 752 field is shown in Figure 2.1

Observing star clusters is advantageous for several reasons. First of all, the stars in the cluster are close together so several stars can be imaged in the same exposure. In addition, the stars in a cluster can range in spectral type from O down to M. By observing a wide variety of spectral types, we were able to gauge the temperature limits of our color index.

The Pleiades and Hyades star clusters are especially good choices for photometric observations because of their proximity to us. The stars in these clusters are bright enough that we can observe a large range of stars, including the fainter late–type stars (Crawford and Perry 1966),(Crawford and Perry 1976). Both clusters have received a lot of attention in the past, so the physical properties of each star have been well determined.

Our catalogue also includes standard stars that have been commonly used in previous photometric systems. These are all bright stars that are scattered throughout the sky and are easily observed from the northern hemisphere. The set of standards we used contains a wide variety of spectral types so we can easily relate them to the full range of spectral types observed in each cluster.

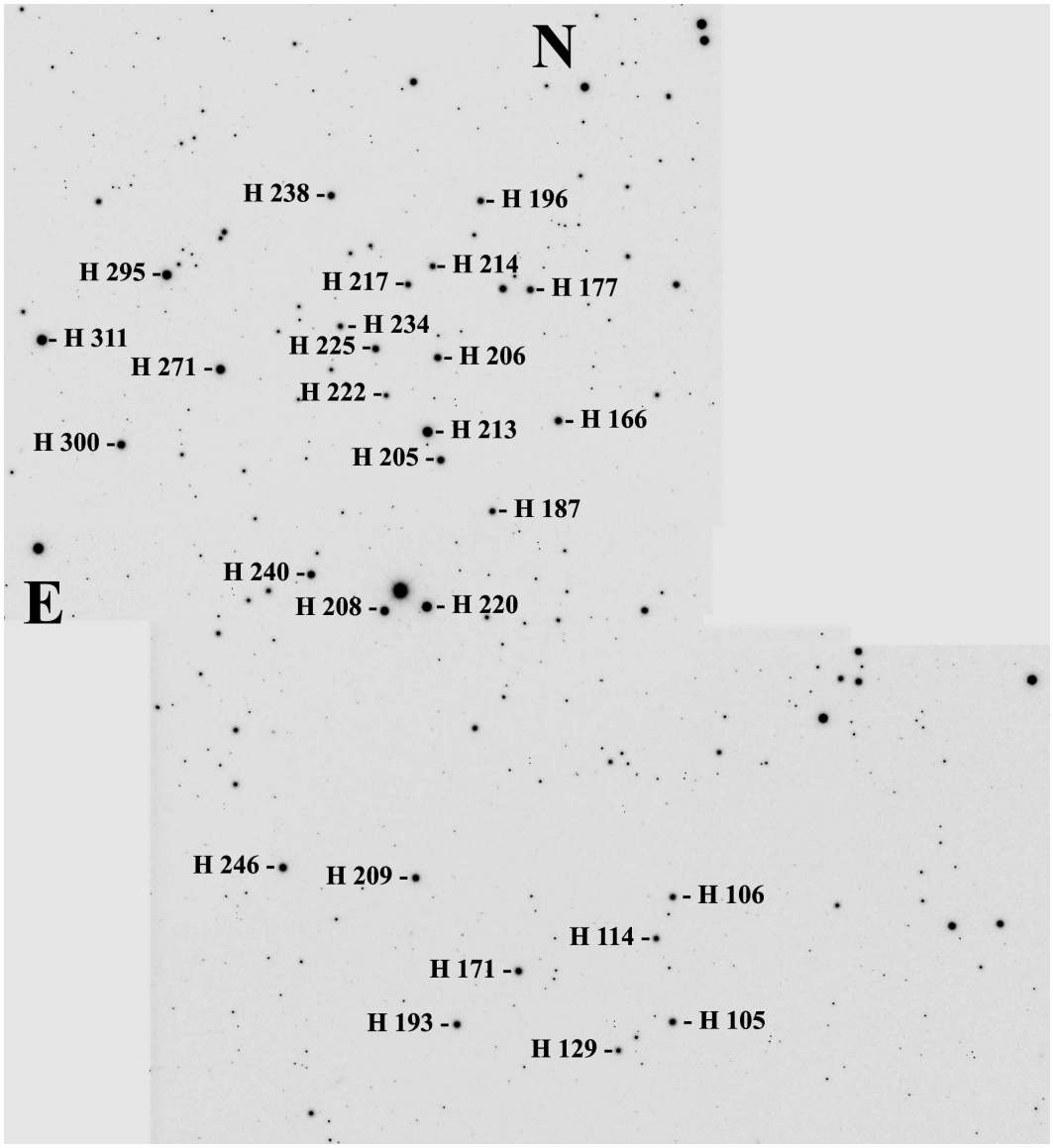


**Figure 2.1:** Stars from NGC 752 used in this catalogue.

## 2.2 Data Collection

Twenty–four nights of observations were obtained during summer 2006/2007, and fall 2007. Each of these nights had to be nearly photometric. We could still work if there were thin clouds in the sky, but if there were scattered clouds near the stars we were observing then we could not do photometric work that night. With very few exceptions, the nights were judged to be photometric. For nights that seemed questionable, we examined the data and found it to be comparable to that of photometric nights and therefore worth retaining.

All observations were obtained at BYU's West Mountain Observatory. We used the 0.31 meter telescope for the summer observations. After the 0.5 meter telescope was installed we were able to use it for the fall 2007 observations. More information on the observatory and telescopes will be given in Sections 2.3.1 and 2.3.2.

While taking our observations we took two exposures in the wide filter, followed by four in the narrow filter, and two more in the wide. This WWNNNNWW palindrome sequence allowed us to immediately measure the quality of our data. If the two sets of wide filter exposures gave similar readings after time had elapsed for the narrow exposures, then we knew we were getting good data. If not, we could immediately see it and determine that the night was not of photometric quality.

## 2.3 Equipment

### 2.3.1 West Mountain Observatory

West Mountain Observatory is the largest observatory in Utah. The observatory is located west of Utah Lake on West Mountain at an elevation of 6850 feet. It currently houses three telescopes: a 0.5 meter RCOS optical tube, a 0.4 meter Meade reflector, and a 0.31 meter RCOS optical tube. The dome where the 0.5 meter telescope was housed is attached to the observatory building (BYU 2008).

West Mountain was the best location to take the observations for our index. Due to its remote location there is little light pollution. That, combined with the good seeing conditions, makes the observatory an excellent location for all-sky photometry. About sixty nights in a given year are apt for such observations (BYU 2008).

### 2.3.2 Telescopes and filters

All summer observations were secured at the 0.31 meter reflector telescope at West Mountain Observatory. This telescope has a focal ratio of 9.22. It is equipped with a SBIG ST-10 XME CCD camera giving a platescale of 0.49 arcsec/pixel and a field of view of 17.9 x 12 arcminutes.

The 0.5 meter reflector was used for fall 2007 observations. Its focal ratio is 8.22. The CCD on this telescope is a STL-1001 E CCD; thus the platescale is 1.20 arcsec/pixel and the field of view is 20.5 x 20.5 arcmin.

**Figure 2.2:** West Mountain Observatory.

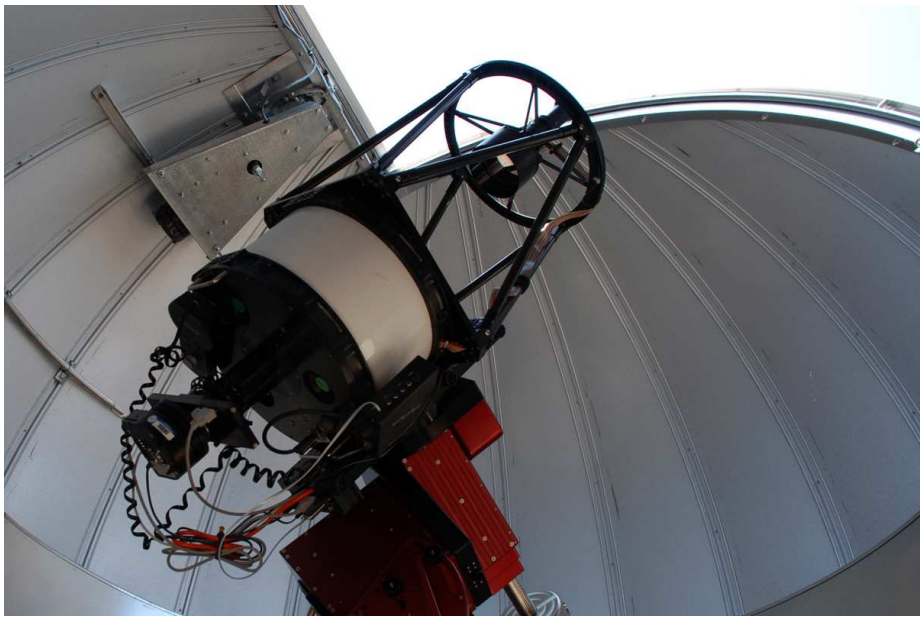

**Figure 2.3:** The 0.31 meter telescope at West Mountain Observatory

This project used a set of H$\alpha$ filters consisting of a narrow bandpass filter and a wide bandpass filter. Both were centered at 6563 Å. The narrow filter spans 30 Å and the wide filter spans 210 Å.

### 2.3.3 Charge-Coupled Devices

Charge coupled devices are the most commonly used detector, mainly because of their high quantum efficiency (QE) compared to that of other detectors. The most sensitive photographic plates had QE of only 10% at most, but generally less. Solid state detectors achieved QE of 20-40%, which was a great improvement, but early CCDs easily matched it. Now modern CCDs have achieved QE of 60% over 2/3 of the spectrum, the peak being 90% (Howell 2000). For our own research we used Santa Barbara Instruments Group Research series CCD housings. For more information on how CCDs work, see Appendix C.

The SBIG ST-10 XME CCD on the 0.31 meter telescope has dimensions 2184 x 1472 pixels. For H$\alpha$ photometry the CCD was binned 2x2 (charge from a 2x2 area

of pixels was read out as if it came from one pixel), so the effective dimensions were 1092 x 732. The pixel size is 6.8 microns (13.6 microns after binning 2x2). With binning, the effective platescale is 0.98 arcsec/pixel.

The CCD on the 0.5 meter telescope is a STL-1001 E CCD. Observations on this telescope were unbinned. The dimensions of the CCD are 1024 x 1024 pixels and the pixel size is 24 microns.

# Chapter 3

# Data Reduction

## 3.1 Calibration frames

### 3.1.1 Bias Frames

A CCD's bias level consists of a number of extra electrons per pixel. To remove this noise we use bias frames, also known as zero frames. These are frames with a zero second exposure length and a closed shutter. This fixes a zero level so we can remove the extra noise that is inherent in the CCD.

The bias level has slight variations that must be accounted for. One bias frame alone cannot capture these variations, so at least ten frames need to be taken. These frames are then averaged and combined into one bias frame. The final frame is used to subtract the bias level noise from the object image (Howell 2000). We commonly use 15-25 bias frames.

### 3.1.2 Dark Frames

Dark frames remove the read noise that is due to the dark current in the CCD. The level of thermal noise from the dark current is dependent on both the CCD temperature and the exposure length. Long exposures and higher temperatures both increase the dark current noise. Dark frames are taken with the shutter closed and with an extended exposure length that is at least equal to that of the object frames. For our own research we took three minute exposures for our dark frames. Once again, it is best to take several dark frames, average them together, and then use the composite image to remove the dark current noise from the object frame (Howell 2000). The composite dark frame can also be calibrated to the time scale of the object frames.

### 3.1.3 Flat Frames

Flat frames are needed to account for the differences in pixel response to the same intensity of light. Pixel response is dependent on both the intensity of the light, as well as the filter used. Therefore, flats must be taken in each filter that will be used that night. To take a flat frame, an exposure of a uniformly lit field is taken. The field should be brighter than any object that will be observed in order to get a high signal to noise ratio.

There are several methods of taking flat frames. One method is to light a screen and mount it in the dome. These are called dome flats. Another method is to take sky flats (exposures of the sky) either at twilight or at dusk. Occasionally, stars end up in sky flat frames. As long as the telescope is moved between each exposure, these stars will not appear in the averaged frame because values that deviate from the mean are rejected in the combining process (Howell 2000). For our research we used sky flats.

## 3.2 Aperture Photometry

After calibrating the images we used the IRAF apphot package to determine the magnitude of each star. This package measures magnitude by first drawing two circles around the image of the star, as shown in Figure 3.1. The blue circle, called the aperture, measures the counts of each pixel in the stellar image plus the sky signal. The red circle is called the annulus and it measures the sky signal. These numbers are then subtracted from each other to give the sky corrected magnitude of the star.

Before using apphot, we needed to choose the size of our aperture. Stars are point sources, but their image is smeared out over several pixels on the CCD chip. The pixels towards the center contain more ADUs than the pixels at the edge of the stellar image. This spread is almost a Gaussian profile and is called the point spread function (PSF). An aperture radius of three full–width half–maximum (FWHM) will

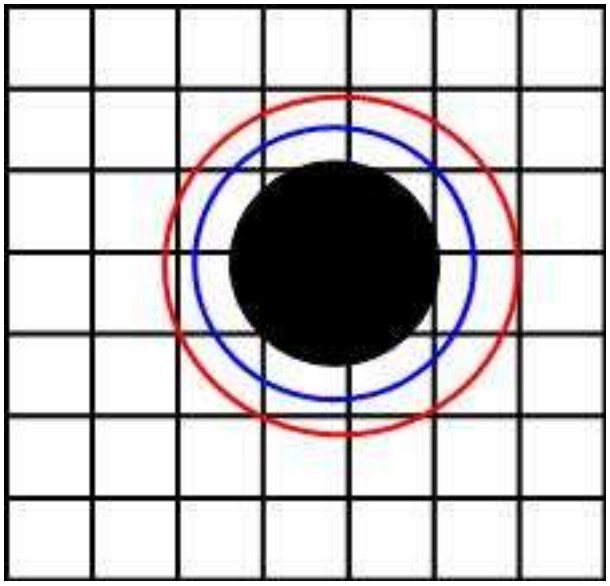

**Figure 3.1:** An example of the aperture and annulus around a star. The aperture is the blue circle and measures the ADU from the stellar image and the sky signal. The annulus is the red circle and it measures only the sky signal.

collect all the photons in the star's image, but we get the best signal–to–noise ratio if the radius is only one FWHM.

We found an aperture radius of thirteen pixels gave the best compromise. This aperture size was large enough to enclose the entire PSF. Because the stars were so bright, the signal-to-noise ratio was already high so a larger aperture did not compromise our results. Because the plate scales of both telescopes were almost equal, the same aperture size was used for observations from both telescopes.

After determining the counts in the stellar image, we had to find out how many of those counts actually came from that star. While the calibrations remove much of the noise from the CCD, they do not remove the sky noise. Sky noise is created by other astronomical objects, cosmic rays, and some CCD noise that the calibration frames did not remove. The annulus measures this noise and is used to remove the noise from the stellar image (Howell 2000).

# Chapter 4

# Data analysis and results

## 4.1 Results

After all the data were reduced, three sets of data were left for calibration to the same system. One set included all the data taken on the 0.31 meter during 2006, another was the data taken on the 0.31 meter in 2007, and the final data set included data taken on the 0.5 meter in 2007. In order to compare data from each set, a zero point was chosen. The zero point selected was the data taken on 9 August 2006, because it contained a significant number of observations that overlapped with those of all the other nights. Each night's observation was then subtracted from that of 9 August 2006. Those differences were averaged and the standard deviation was found. If the standard deviation was significantly smaller than the average, then applied average was applied as a correction to the night. For our data no corrections were needed. Our results are shown in Table 4.1.

**Table 4.1:** Results

| Star | Spectral Type * | H$\alpha$ | Standard Deviation | Observations |
|---|---|---|---|---|
| BD+37 3404 | K5 | 2.070 | 0.0104 | 13 |
| BD+37 3405 | F5 | 2.159 | 0.0110 | 13 |
| HD 24097 | K0 | 2.083 | 0.0023 | 4 |
| HD 24132 | F2V | 2.193 | 0.0015 | 4 |
| HD 94028 | F4V | 2.141 | – | 1 |
| HD 109995 | A0 | 2.287 | 0.0118 | 12 |
| HD 140283 | F3 | 2.120 | 0.0185 | 11 |
| HD 161817 | A2 | 2.226 | 0.0105 | 16 |
| HD 283060 | K2 | 2.068 | 0.0027 | 4 |
| HR 493 | K1V | 2.087 | 0.0113 | 6 |
| HR 675 | A2V | 2.302 | 0.0089 | 7 |
| HR 1144 | B8V | 2.119 | 0.0071 | 8 |
| HR 3928 | F6V | 2.174 | 0.0169 | 6 |
| HR 3951 | G3V | 2.125 | 0.0066 | 4 |
| HR 4456 | B4V | 2.190 | – | 1 |

Table 4.1 – Continued

| Star | Spectral Type | H$\alpha$ | Standard Deviation | Observations |
|---|---|---|---|---|
| HR 5011 | G0V | 2.142 | 0.0161 | 7 |
| HR 5270 | F8IV | 2.093 | 0.0166 | 11 |
| HR 5936 | F0IV | 2.205 | 0.0119 | 19 |
| HR 5968 | G0V | 2.123 | 0.0104 | 19 |
| HR 7253 | F0III | 2.240 | 0.0140 | 20 |
| HR 7462 | K0V | 2.097 | 0.0196 | 9 |
| HR 7469 | F4V | 2.221 | 0.0156 | 4 |
| HR 7503 | G1.5V | 2.133 | 0.0119 | 20 |
| HR 7504 | G3V | 2.132 | 0.0121 | 20 |
| HR 7534 | F7V | 2.176 | 0.0157 | 11 |
| HR 7560 | F8V | 2.148 | 0.0168 | 20 |
| HR 7610 | A2IV | 2.324 | 0.0149 | 20 |
| HR 8085 | K5V | 2.055 | 0.0149 | 11 |
| HR 8086 | K7V | 2.046 | 0.0146 | 11 |
| HR 9088 | G5V | 2.106 | 0.0122 | 6 |
| Tr 10 | A4Vn | 2.295 | 0.0148 | 9 |
| Tr 19 | F5V | 2.182 | 0.0133 | 9 |
| Tr 49 | F2V | 2.195 | 0.0160 | 9 |
| Tr 62 | A8 | 2.309 | 0.0086 | 8 |
| Tr 76 | F8V | 2.083 | 0.0099 | 4 |
| Tr 82 | Am | 2.237 | 0.0120 | 2 |
| Tr 86 | F6V | 2.156 | 0.0172 | 9 |
| Tr 90 | F6 | 2.160 | 0.0186 | 9 |
| Tr 114 | F5 | 2.160 | 0.0121 | 8 |
| Tr 118 | F5 | 2.171 | 0.0137 | 9 |
| Tr 127 | F8/9V | 2.144 | 0.0115 | 10 |
| Tr 130 | A4V | 2.304 | 0.0120 | 10 |
| Tr 132 | G5V | 2.120 | 0.0160 | 10 |
| Tr 144 | A2m | 2.287 | 0.0100 | 9 |
| Tr 145 | A0p | 2.296 | 0.0170 | 10 |
| Tr 146 | A0 | 2.282 | 0.0292 | 8 |
| Tr 162 | F6V | 2.156 | 0.0143 | 9 |
| Tr 183 | A4V | 2.320 | 0.0135 | 10 |
| HD 23156 | A7V | 2.270 | 0.0045 | 3 |
| HD 23157 | A5V | 2.241 | 0.0148 | 14 |
| HD 23158 | F5V | 2.156 | 0.0077 | 14 |
| HD 23194 | A5V | 2.308 | 0.0046 | 4 |
| HD 23246 | A8V | 2.245 | 0.0032 | 4 |
| HD 23247 | A2 | 2.192 | 0.0013 | 4 |
| HD 23289 | F3V | 2.201 | 0.0112 | 4 |
| HD 23325 | Am | 2.275 | 0.0016 | 3 |
| HD 23326 | F2V | 2.192 | 0.0081 | 4 |
| HD 23339 | G5 | 2.117 | 0.0040 | 4 |
| HD 23353 | G0 | 2.117 | 0.0137 | 4 |
| HD 23410 | A0V | 2.300 | 0.0056 | 7 |
| HD 23464 | G0V | 2.122 | 0.0090 | 4 |
| HD 23479 | A7V | 2.226 | 0.0044 | 4 |
| HD 23489 | A2V | 2.308 | 0.0171 | 4 |
| HD 23511 | F4V | 2.175 | 0.0083 | 4 |

Table 4.1 – Continued

| Star | Spectral Type | H$\alpha$ | Standard Deviation | Observations |
|---|---|---|---|---|
| HD 23513 | F5V | 2.173 | 0.0051 | 8 |
| HD 23585 | F0V | 2.232 | 0.0084 | 6 |
| HD 23607 | A7V | 2.275 | 0.0138 | 12 |
| HD 23608 | F3V | 2.156 | 0.0159 | 12 |
| HD 23629 | A0V | 2.307 | 0.0089 | 11 |
| HD 23631 | G5V | 2.289 | 0.0048 | 6 |
| HD 23632 | A1V | 2.316 | 0.0031 | 4 |
| HD 23872 | A1V | 2.294 | 0.0096 | 8 |
| HD 23948 | A1V | 2.336 | 0.0056 | 8 |
| HD 23886 | A5V | 2.291 | 0.0078 | 2 |
| HD 23912 | F3V | 2.179 | 0.0114 | 7 |
| HD 23924 | A7 | 2.299 | 0.0125 | 7 |
| VB 6 | F4V | 2.207 | 0.0078 | 6 |
| VB 10 | G0 | 2.130 | – | 1 |
| VB 15 | G5 | 2.119 | 0.0123 | 7 |
| VB 17 | G5 | 2.062 | 0.0057 | 5 |
| VB 19 | F8V | 2.159 | 0.0121 | 6 |
| VB 53 | F4V | 2.196 | 0.0195 | 3 |
| VB 64 | G2V | 2.11 | 0.0186 | 4 |
| VB 66 | F8 | 2.117 | – | 1 |
| VB 75 | F8 | 2.160 | 0.0131 | 3 |
| VB 89 | F4V | 2.120 | – | 1 |
| H 105 | F3IV | 2.175 | 0.0102 | 8 |
| H 106 | F2III | 2.188 | 0.0056 | 8 |
| H 114 | F2III | 2.182 | 0.0156 | 9 |
| H 126 | F3.4IV | 2.168 | 0.0082 | 7 |
| H 129 | F2V | 2.187 | 0.0150 | 8 |
| H 166 | F0III | 2.180 | 0.0114 | 14 |
| H 171 | F3IV | 2.165 | 0.0124 | 11 |
| H 177 | F4.5IV | 2.154 | 0.0149 | 14 |
| H 187 | F3V | 2.177 | 0.0139 | 14 |
| H 193 | F2 | 2.201 | 0.0075 | 11 |
| H 196 | F3.5IV | 2.172 | 0.0141 | 11 |
| H 205 | F3IV-V | 2.173 | 0.0117 | 14 |
| H 206 | F4.5IV | 2.157 | 0.0105 | 14 |
| H 208 | K1IV | 2.060 | 0.0179 | 14 |
| H 209 | B9.5V | 2.319 | 0.0112 | 11 |
| H 213 | G9III | 2.065 | 0.0206 | 14 |
| H 214 | F2IV | 2.187 | 0.0188 | 14 |
| H 217 | F2.5IV | 2.174 | 0.0153 | 14 |
| H 220 | K0V | 2.078 | 0.0111 | 14 |
| H 222 | F2.5IV | 2.186 | 0.0149 | 14 |
| H 225 | F5V | 2.149 | 0.0089 | 14 |
| H 234 | F4IV-V | 2.182 | 0.0148 | 14 |
| H 238 | F4.5IV | 2.182 | 0.0077 | 12 |
| H 240 | F5V | 2.161 | 0.0130 | 12 |
| H 246 | K0V | 2.071 | – | 1 |
| H 271 | F1V | 2.209 | 0.0096 | 14 |
| H 295 | G8III | 2.078 | 0.0076 | 12 |

Table 4.1 – Continued

| Star | Spectral Type | H$\alpha$ | Standard Deviation | Observations |
|---|---|---|---|---|
| H 300 | F3III-IV | 2.191 | 0.0120 | 8 |
| H 311 | G9III | 2.071 | 0.0199 | 10 |

[a]Spectral types for stars from NGC 752 were obtained from Mermilliod and Paunzen(2009). All others were obtained from Simbad(2009)

After calibrating the data, the final values for the H$\alpha$ color index for each star were found. For each star, over all the nights it was observed, the H$\alpha$ value was averaged and the standard deviation was found. A standard deviation below 0.02 was desirable. If a star's standard deviation exceeded this, it was investigated further for possible reasons.

The most common reason for excessive standard deviation was the star was too bright or too dim for the telescope. The 0.31 meter telescope gave precise results for stars between 3rd and 9th magnitudes while the 0.5 meter telescope, being larger, was capable of observing fainter magnitudes. Its range was 4th–11th magnitude stars.

Once the stars that were too bright or too dim for the telescopes were removed there remained a couple of stars that still had a high standard deviation. One of these stars is Tr 146. Further investigation revealed that Tr 146 is a variable star so higher errors are to be expected.

The second star with high errors is H 213. Preliminary examinations show no obvious reason for these high errors, so further investigation is needed.

The last step in testing the data was to plot it. The first plots compare the visible magnitude to the H$\alpha$ index of each star in the star clusters. This is the same as plotting temperature versus H$\alpha$ index. This is because the stars in a given cluster are roughly the same distance away, so the brighter stars must have a higher temperature. These plots are shown in Figure 4.1.

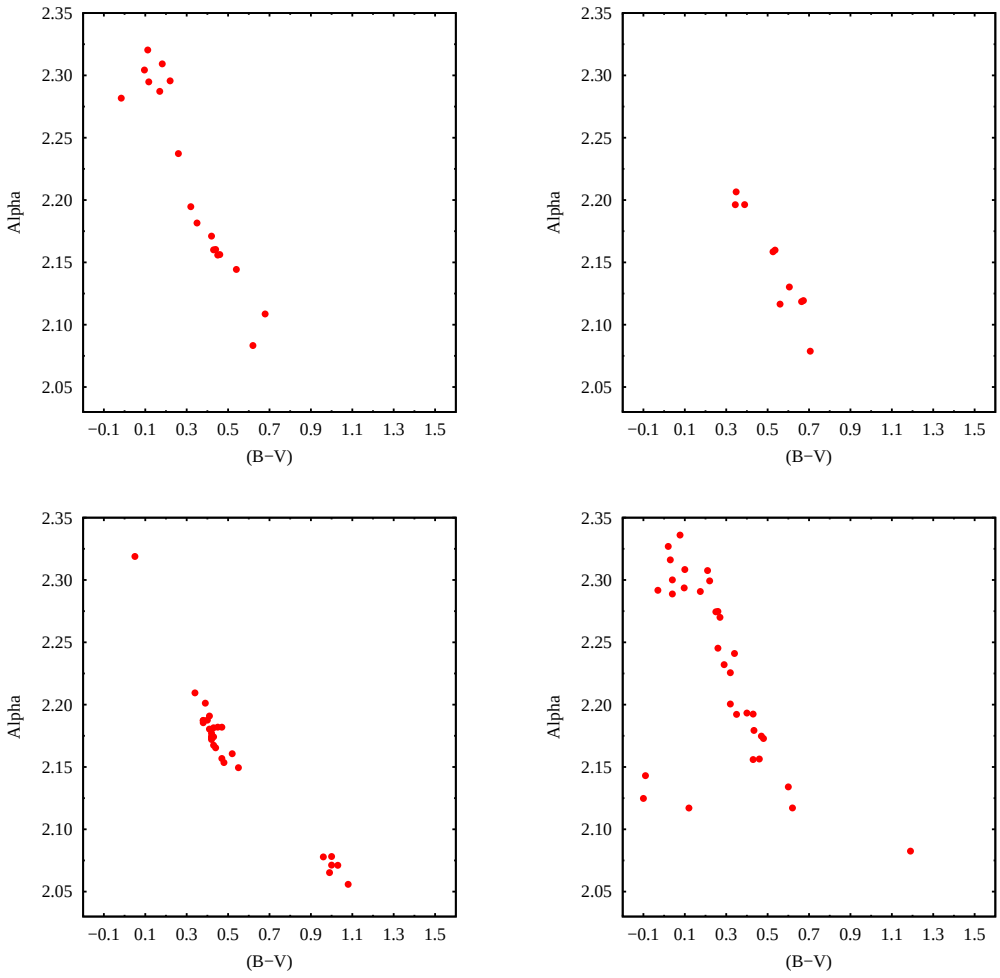


**Figure 4.1:** Visible magnitudes versus H$\alpha$ index for a) Coma, b) Hyades, c) NGC 752, d) Pleiades star clusters. As H$\alpha$ index increases so does the temperature as indicated by magnitude. The only exceptions are the B stars in the Pleiades. These exceptions are expected, as hot B stars have weak hydrogen lines. The NGC 752 graph looks different because the stars are not all at the same distance.

Both the Coma and Hyades cluster graphs show that hotter stars (stars with a lower magnitude) have a higher H$\alpha$ index. This is exactly the result that was expected. (See Section 1.3.3 for a discussion on how hydrogen line strength relates to temperature.)

Alternatively, the trend in NGC 752 is not at all what was expected. The most likely cause of this is that not all the stars are actually a part of the star cluster. Several of the F stars have a higher magnitude than some of the K and G stars, indicating that they are farther away. Additionally the B star, Hn 209, has a higher magnitude than Hn 311, a G star. If a B star and G star are at the same distance, the B star would have a much lower magnitude. This indicates that Hn 209 is farther away than the other stars we observed.

At first glance, the graph of the Pleiades cluster appears incorrect because there are a few outliers in the top left quadrant. Examination of these stars shows they are where they should be. These stars are the hot B stars. Recall from Section 1.3.3 that B stars are so hot that they ionize hydrogen and thus they have weak hydrogen lines. This is precisely what the graph shows. These B stars have a low magnitude because they are hot and they have a small H$\alpha$ color index.

The H$\alpha$ color index was also compared to the B$-$V color index. This is similar to previous plots because the B$-$V index is a temperature indicator. The B$-$V color index is independent of distance, so all of the stars were plotted in one graph. This graph contains spectral types B–K. A graph that looks like Figure 1.3 was expected. Our results are shown in Figure 4.2.

With a few exceptions, our graph is similar to Figure 1.3. Fortunately, all exceptions can be explained. First of all, HR 1144, HD 23463, and HD 23630 are all reddened B stars. Because of reddening effects, the B-V color index of these stars is higher than it would be without reddening. If the effects of reddening were removed the stars would slide left on the plot and lie on the curve.

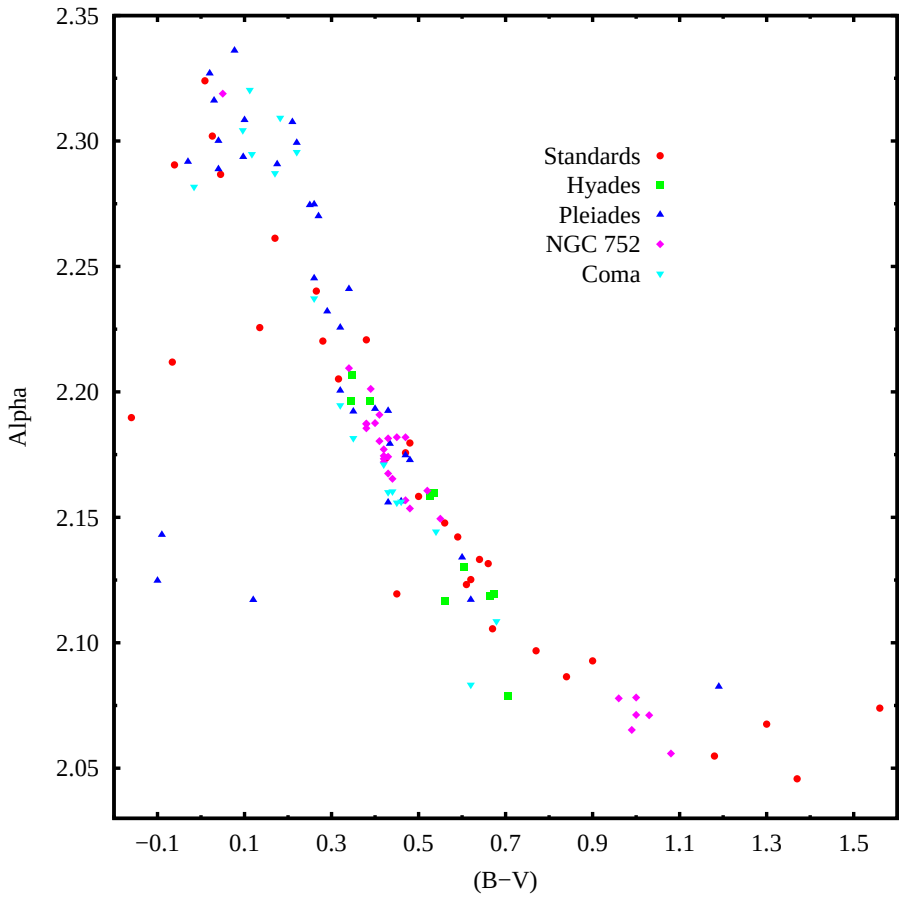


**Figure 4.2:** B-V versus H$\alpha$ graph for all stars. This graph is similar to Figure 1.3. Type A stars have the highest H$\alpha$ index, while B and K stars have weaker indices. The H$\alpha$ index of F and G stars lies in between.

The other outlying standard stars are HD 140283 and HD 161817. These stars are emission stars. The emission will affect the strength of the H$\alpha$ line so no accurate correlation between H$\alpha$ line strength and temperature can be made for these stars.

Figure 4.2 shows more scattering at B-V indices greater than 1.1. These are the coolest K stars we observed. The high degree of scattering may indicate that the limit of the H$\alpha$ color index has been reached and the H$\alpha$ line of these stars is too weak for H$\alpha$ photometric work.

## 4.2 Conclusion

So far our method yields good results. We have found that our errors are low, except for a known variable star and two other stars that require further investigation. Our numbers gave the curves we expected to receive. The only exception is the plot of V magnitude versus H$\alpha$ index for NGC 752. This exception is a result of the varying distances to the stars and is not caused by poor results. Additionally, our index includes stars that range from the B spectral type down to K types. This is a much wider range than that of the H$\beta$ index.

This project's results were independent of the telescopes. No corrections from night to night or telescope to telescope needed to be applied. Therefore, this method can be used in other projects and yield similar results. We hope others will take advantage of our work and use the H$\alpha$ color index because it is more advantageous than dual wavelength indices and the H$\beta$ index.

## References


Roger A. Freedman, Universe, 7th ed. (W.H. Freeman and Company, New York, 2005), pp. 98, 112, 420-424, 447, 470, 378-389.

Michael Zeilik, Stephen A. Gregory, Introductory Astronomy & Astrophysics, 4th ed. (Saunders College Publishing, New York, 1998), pg. 255-259, 229-231, 227.

E.H.Olsen,"Four-colour *uvby* and H$\beta$ photometry of A5 to G0 stars brighter than $8^m.3$," Astron. Astrophys. Suppl. Ser. **54,** 55-134 (1983).

M.S. Bessell, "*UBVRI* Photometry II: The Cousins *VRI* System, its Temperature and Absolute Flux Calibration, and Relevance for Two-Dimensional Photometry," Publications of the Astronomical Society of the Pacific **91**(543), 589-607, (1979).

Edwin Budding, An Introduction to Astronomical Photometry (Cambridge University Press, 1993), pp. 61, 80

Michael Fowler,"Spectra," http://www.physics.byu.edu/Undergraduate/Docs/thesis.pdf (Accessed July 31, 2008).

D.L. Crawford, Jeannette Mander, "Standard Stars for Photoelectric H$\beta$ Photometry," The Astronomical Journal **71**(2), 114-118 (1966).

D.W. Peat, "H$\alpha$ Photometry of Late-Type Stars, I. F,G, and K Type Stars North of the Equator," Monthly Notices of the Royal Astronomical Society **128**(6), 435-473, (1963).

J. Dachs and T. Schmidt-Kaler, "Standard Stars for Photoelectric H$\alpha$ Line Photometry," Astron. Astrophys. Suppl. **21,** 81-97, (1975).

D.L. Crawford, C.L. Perry, "Four-Color and H$\beta$ Photometry of Open Clusters. I. The Hyades," The Astronomical Journal **71**(3), 206-214 (1966).

D.L. Crawford, C.L. Perry, "Four-color and H$\beta$ for open cluster. XI. The Pleiades," The Astronomical Journal **81**(6), (1976).

BYU Physics-Astronomy Department, "West Mountain Observatory," http://astronomy.byu.edu/wmo.php (Accessed 6 August 2008).

Steve B. Howell, Handbook of CCD Astronomy, (Cambridge University Press, 2000) pp 5, 8-11, 50-60, 80

Arne A. Henden, Ronald H. Kaitchuck, Astronomical Photometry (Van Nostrand Reinhold Company Inc., 1982), pp 40

Michael D. Joner, Benjamin J. Taylor, "Homogeneous photometry for the Hyades: scale-factor and zero-point tests of previously published BV(RI)$_C$ Photometry," The Astronomical Journal **132**(111-116), (2006).

Jean-Claude Mermilliod, Ernst Paunzen, Webda, http://www.univie.ac.at/webda/ (Accessed 12 April 2009)

Simbad Astronomical Database, http://simbad.u-strasbg.fr/simbad/ (Accessed 12 April 2009)

Benjamin J. Taylor, Michael D. Joner, "The Consistency of Strömgren-Beta Photometry for Northern Galactic Clusters. I. The Hyades and Coma," Publications of the Astronomical Society of the Pacific **104**(911-922), (1992).

# Appendix A

## Stellar Data

The following are tables listing relevant data of the stars we observed.

**Table A.1:** Target star data

| Star | Spectral Type* | V† | B-V‡ | *b-y*§ | Exposure Time(s) N | W |
|---|---|---|---|---|---|---|
| BD+37 3404 | K5 | 9.44 | 1.56 | – | 90 | 20 |
| BD+37 3405 | F5 | 9.45 | 0.48 | – | 90 | 20 |
| HD 24097 | K0 | 9.37 | 1.19 | – | 75 | 15 |
| HD 24132 | F2V | 8.84 | 0.40 | 0.254 | 75 | 15 |
| HD 94028 | F4V | 8.23 | 0.47 | 0.336 | 70 | 20 |
| HD 109995 | A0 | 7.60 | 0.05 | 0.047 | 40 | 8 |
| HD 140283 | F3 | 7.24 | 0.45 | 0.371 | 110 | 30 |
| HD 161817 | A2 | 6.99 | 0.14 | 0.128 | 40 | 6 |
| HD 283060 | K2 | 10.80 | 1.30 | – | 75 | 15 |
| HR 493 | K1V | 5.20 | 0.84 | 0.497 | 10 | 2 |
| HR 675 | A2V | 5.29 | 0.03 | 0.009 | 10 | 2 |
| HR 1144 | B8V | 5.65 | -0.07 | -0.029 | 10 | 2 |
| HR 3928 | F6V | 5.12 | 0.43 | 0.460 | 10 | 2 |
| HR 3951 | G3V | 5.40 | 0.62 | 0.415 | 10 | 2 |
| HR 4456 | B4V | 5.95 | -0.16 | -0.075 | 15 | 3 |
| HR 5011 | G0V | 5.22 | 0.59 | 0.372 | 6 | 1 |
| HR 5270 | F8IV | 6.20 | 0.90 | 0.649 | 10 | 2 |
| HR 5936 | F0IV | 5.44 | 0.32 | 0.231 | 6 | 1 |
| HR 5968 | G0V | 5.40 | 0.61 | 0.391 | 6 | 1 |
| HR 7253 | F0III | 5.53 | 0.27 | 0.178 | 6 | 1 |
| HR 7462 | K0V | 4.70 | 0.77 | 0.479 | 5 | 1 |
| HR 7469 | F4V | 4.48 | 0.38 | 0.267 | 5 | 1 |
| HR 7503 | G1.5V | 5.96 | 0.64 | 0.408 | 6 | 1 |
| HR 7504 | G3V | 6.20 | 0.66 | 0.414 | 6 | 1 |
| HR 7534 | F7V | 4.99 | 0.47 | 0.312 | 5 | 1 |
| HR 7560 | F8V | 5.10 | 0.56 | 0.354 | 6 | 1 |
| HR 7610 | A1IV | 5.29 | 0.00 | -0.005 | 6 | 1 |
| HR 8085 | K5V | 5.21 | 1.18 | – | 5 | 1 |
| HR 8086 | K7V | 6.03 | 1.37 | – | 5 | 1 |
| HR 9088 | G5V | 5.75 | 0.67 | 0.435 | 5 | 1 |
| Tr 10 | A4V | 6.00 | 0.12 | 0.070 | 15 | 3 |
| Tr 19 | F5V | 8.09 | 0.35 | 0.265 | 50 | 10 |
| Tr 49 | F2V | 7.87 | 0.32 | 0.240 | 50 | 10 |
| Tr 62 | A8 | 6.24 | 0.182 | 0.076 | 15 | 3 |
| Tr 76 | F8V | 9.00 | 0.62 | 0.358 | 50 | 10 |

Table A.1 – Continued

| Star | Spectral Type | V | B-V | b-y | Exposure Time(s) N | W |
|---|---|---|---|---|---|---|
| Tr 82 | Am | 7.38 | 0.26 | 0.170 | 50 | 10 |
| Tr 86 | F6V | 8.50 | 0.45 | 0.302 | 50 | 10 |
| Tr 90 | F6 | 8.54 | 0.44 | 0.304 | 50 | 10 |
| Tr 114 | F5 | 8.56 | 0.43 | 0.304 | 50 | 10 |
| Tr 118 | F5 | 8.34 | 0.42 | 0.290 | 50 | 10 |
| Tr 127 | F8/9V | 8.80 | 0.54 | – | 60 | 10 |
| Tr 130 | A4V | 4.97 | 0.10 | 0.051 | 6 | 1 |
| Tr 132 | G5V | 9.91 | 0.68 | 0.424 | 60 | 10 |
| Tr 144 | A2m | 6.54 | 0.17 | 0.099 | 15 | 3 |
| Tr 145 | A0p | 6.65 | -0.02 | 0.123 | 15 | 3 |
| Tr 146 | A0 | 5.29 | -0.118 | -0.057 | 15 | 3 |
| Tr 162 | F6V | 8.54 | 0.46 | 0.301 | 50 | 10 |
| Tr 183 | A4V | 6.27 | 0.11 | 0.055 | 15 | 3 |
| HD 23156 | A7V | 8.22 | 0.27 | 0.149 | 75 | 15 |
| HD 23157 | A5V | 7.95 | 0.35 | 0.213 | 75 | 15 |
| HD 23158 | F5V | 9.58 | 0.46 | 0.335 | 75 | 15 |
| HD 23194 | A5V | 8.07 | 0.21 | 0.118 | 75 | 15 |
| HD 23246 | A8V | 8.18 | 0.26 | 0.171 | 75 | 15 |
| HD 23247 | A2 | 9.06 | 0.43 | 0.307 | 75 | 15 |
| HD 23289 | F3V | 9.01 | 0.32 | 0.263 | 75 | 15 |
| HD 23325 | Am | 8.70 | 0.26 | 0.219 | 75 | 15 |
| HD 23326 | F2V | 8.99 | 0.35 | 0.250 | 75 | 15 |
| HD 23339 | A2V | 9.24 | 0.12 | – | 75 | 15 |
| HD 23353 | G0 | 8.48 | 0.62 | – | 75 | 15 |
| HD 23410 | A0V | 6.89 | 0.04 | – | 30 | 5 |
| HD 23464 | G0V | 8.67 | 0.62 | 0.377 | 30 | 5 |
| HD 23479 | A7V | 7.96 | 0.32 | 0.208 | 75 | 15 |
| HD 23489 | A2V | 7.38 | 0.10 | 0.058 | 75 | 15 |
| HD 23511 | F4V | 9.28 | 0.47 | 0.311 | 75 | 15 |
| HD 23513 | F5V | 9.38 | 0.48 | 0.315 | 30 | 5 |
| HD 23585 | F0V | 8.38 | 0.29 | 0.186 | 15 | 3 |
| HD 23607 | A7V | 8.26 | 0.25 | 0.153 | 15 | 3 |
| HD 23608 | F3V | 8.72 | 0.43 | 0.296 | 15 | 3 |
| HD 23629 | A0V | 6.28 | 0.02 | 0.000 | 15 | 3 |
| HD 23631 | G5V | 7.30 | 0.04 | 0.048 | 50 | 10 |
| HD 23632 | A1V | 7.02 | 0.03 | 0.013 | 50 | 10 |
| HD 23872 | A1Va n | 7.51 | 0.01 | 0.055 | 20 | 4 |
| HD 23886 | A5V | 7.96 | 0.18 | 0.093 | 20 | 4 |
| HD 23912 | F3V | 9.14 | 0.43 | 0.290 | 75 | 15 |
| HD 23924 | A7m | 8.13 | 0.22 | 0.116 | 75 | 15 |
| VB 6 | F4V | 5.95 | 0.35 | – | 10 | 2 |
| VB 10 | G0 | 7.81 | 0.61 | 0.374 | 10 | 5 |
| VB 15 | G5 | 8.05 | 0.66 | 0.401 | 40 | 8 |
| VB 17 | G5 | 8.42 | 0.71 | – | 35 | 7 |
| VB 19 | F8V | 7.08 | 0.53 | 0.332 | 20 | 4 |
| VB 53 | F4V | 5.97 | 0.39 | 0.247 | 12 | 3 |
| VB 64 | G2V | 8.10 | 0.67 | 0.410 | 40 | 8 |

Table A.1 – Continued

| Star | Spectral Type | V | B-V | b-y | Exposure Time(s) N | W |
|---|---|---|---|---|---|---|
| VB 66 | F8 | 7.49 | 0.56 | – | 25 | 5 |
| VB 75 | F | 6.57 | 0.31 | – | 15 | 3 |
| VB 89 | F4V | 6.00 | 0.34 | – | 15 | 3 |
| H 105 | F3IV | 10.22 | 0.42 | 0.272 | 90 | 20 |
| H 106 | F2III | 10.48 | 0.40 | 0.244 | 90 | 20 |
| H 114 | F2III | 10.67 | 0.47 | – | 90 | 20 |
| H 126 | F3.4IV | 10.08 | 0.43 | 0.283 | 90 | 20 |
| H 129 | F2V | 10.86 | 0.38 | 0.151 | 90 | 20 |
| H 166 | F0III | 9.81 | 0.41 | 0.261 | 90 | 20 |
| H 171 | F3IV | 10.16 | 0.44 | 0.281 | 90 | 20 |
| H 177 | F4.5IV | 10.15 | 0.48 | 0.323 | 90 | 20 |
| H 187 | F3V | 10.41 | 0.42 | 0.284 | 90 | 20 |
| H 193 | F2 | 10.17 | 0.39 | 0.242 | 90 | 20 |
| H 196 | F3.5 | 10.24 | 0.42 | 0.279 | 90 | 20 |
| H 205 | F3IV-V | 10.94 | 0.42 | 0.280 | 90 | 20 |
| H 206 | F4.5IV | 10.01 | 0.47 | 0.145 | 90 | 20 |
| H 208 | K1IV | 8.94 | 1.08 | 0.664 | 90 | 20 |
| H 209 | B9.5V | 9.70 | 0.05 | 0.022 | 90 | 20 |
| H 213 | G9III | 9.01 | 0.99 | 0.622 | 90 | 20 |
| H 214 | F2IV | 10.44 | 0.38 | – | 90 | 20 |
| H 217 | F2.5IV | 10.41 | 0.43 | 0.278 | 90 | 20 |
| H 220 | K0V | 9.58 | 1.00 | 0.604 | 90 | 20 |
| H 222 | F2.5IV | 10.94 | 0.38 | 0.256 | 90 | 20 |
| H 225 | F5V | 10.15 | 0.55 | – | 90 | 20 |
| H 234 | F4IV-V | 10.66 | 0.43 | 0.289 | 90 | 20 |
| H 238 | F4.5IV | 9.95 | 0.45 | 0.299 | 90 | 20 |
| H 240 | F5V | 9.74 | 0.52 | – | 90 | 20 |
| H 246 | K0V | 10.09 | 1.00 | – | 90 | 20 |
| H 271 | F1V | 9.12 | 0.34 | – | 90 | 20 |
| H 295 | G8III | 9.29 | 0.96 | 0.597 | 90 | 20 |
| H 300 | F3III-IV | 9.58 | 0.41 | 0.271 | 90 | 20 |
| H 311 | G9III | 9.04 | 1.03 | 0.641 | 90 | 20 |

[a]Spectral types for stars from NGC 752 were obtained from Mermilliod and Paunzen(2009). All others were obtained from Simbad(2009)

[b]Magnitudes for stars from NGC 752 were obtained from Mermilliod and Paunzen(2009). All others were obtained from Simbad(2009)

[c]The B-V color indices for stars from NGC 752 were obtained from Mermilliod and Paunzen(2009). All others were obtained from Simbad(2009)

[d]The *b-y* color indices for stars from NGC 752 were obtained from Mermilliod and Paunzen(2009). Indices for stars in the Pleiades were obtained from Crawford and Perry(1976). Information on Hyades stars was obtained from Joner and Taylor(2006) and all others were obtained from Taylor and Joner(1992).

# Appendix B

## Balmer Discontinuity

The Balmer spectrum consists of a series of absorption lines corresponding to electron jumps from the n=2 level to higher levels. The lowest energy line corresponds to a jump from n=2 to n=3. A photon with wavelength 6563 Å must be absorbed for this transition to happen. To make a larger jump, the electron must have more energy to make the transition so it absorbs photons of shorter wavelengths.

Because the energy difference between energy levels decreases as the energy levels increase, these lines are spaced more closely at shorter wavelengths than they are at longer wavelengths. As they approach the Balmer limit (located at 3647 Å), the absorption lines merge together. Because there are so many absorption lines, the continuum level drops. This drop is known as the Balmer discontinuity (Henden 1982).

The U–B color index uses the Balmer discontinuity to determine a star's spectral type. The strength of the Balmer discontinuity in a star's spectrum depends on that star's temperature, which is related to its spectral type. Balmer lines are most dominant in spectral type A stars, so they will have the strongest discontinuity. The U filter straddles the Balmer discontinuity, so the star's magnitude as measured through the U filter depends on the strength of the Balmer discontinuity (Henden 1982).

One advantage of the Strömgren *ubvy* system is that it provides a way to measure the Balmer discontinuity without the effects of line blanketing. Measurements through the $u$ filter contain both blanketing and Balmer discontinuity effects. The $v$ filter contains effects only from line blanketing. Line blanketing effects are about half as strong in the $v$ filter as in the $u$ filter. The index $c_1$ can be written as

$$c_1 = (u - 2\mathrm{v} + \mathrm{b}) \tag{B.1}$$

(Henden 1982).

Subtracting the $2v$ term from the u term cancels effects from line blanketing and only the Balmer discontinuity effects are left. While Equation (B.1) is correct, $c_1$ is usually expressed as

$$c_1 = (u - v) - (v - b) \tag{B.2}$$

(Henden 1982).

# Appendix C

## Charge Coupled Devices

The following information is a brief description of how CCDs work. It is included to allow the reader to better understand our data reduction methods. This is in no way meant to be a comprehensive description of CCDs. For more information on CCDs the reader is referred to Howell (2000).

To understand our data reduction methods, one must first have a basic understanding of how CCDs work. For example, our use of calibration frames depends on the inherent noise within a CCD. Additionally, the way the CCD collects photons determines how we will later count those photons. The following brief description of how CCDs work will allow the reader to understand why we used our particular data reduction method.

CCDs count photons by collecting and counting the electrons that the photons excite. Every CCD contains a silicon chip that is divided into smaller regions called pixels. Silicon's bandgap is 1.14 eV, so it will absorb photons with wavelengths between 3000 and 11 000 Å. This excites a valence electron into the conduction band where a series of gates hold it in place (Howell 2000).

After the electrons are collected they must be read out. Following the exposure the electrons are transferred row by row to a device called the output shift register and finally to the output electronics. Here, the charge in each pixel is measured as a voltage, which is then converted into an output digital number. This number is called either the counts or the analog-to-digital units (ADUs). A CCD's gain is the amount of voltage required to produce one ADU (Howell 2000). The higher the ADU in a pixel, the brighter that pixel will appear in the final image.

Although electrons are far better than any other detector, they are not without problems. Namely, not all of the electrons in the conduction band were excited by

incoming photons. Thermal motions in the CCD itself excite electrons and there is no way to distinguish these electrons from the others. The number of extra electrons per pixel is called the read noise.

Any CCD whose temperature is above absolute zero will have some degree of read noise. The best way to reduce this noise is to keep the CCD as cold as possible. Our CCDs were thermoelectrically cooled to temperatures between $-15\,^{\circ}\mathrm{C}$ and $-25\,^{\circ}\mathrm{C}$. Even with cooling there is still some thermal noise in the final readout. Various calibration frames can be used to eliminate most of the extra noise (Howell 2000). See Section 3.1 for more information on calibration frames.

## Index


annulus, 20, 21
aperture, 20, 21
apphot package, 20, 21
atmospheric extinction, 6, 7

Balmer discontinuity, 12, 35, 36
Balmer series, 8
Bohr model, 7

calibration frames, 38
    bias, 19
    dark, 19
    flat, 20
charge coupled device (CCD), 11, 17, 19, 37, 38
    on 0.31 meter telescope, 18
    on 0.5 meter telescope, 18
color
    intrinsic, 6
    quantification of, 4
    temperature dependence of, 4
color index
    dual wavelength, 4–6, 10
    H$\beta$, 11
    single wavelength, 8, 10
    Strömgren, 5, 35, 36
    U–B, 35
    UBV, 5

hydrogen line, 8
    advantage of H$\alpha$ over H$\beta$, 11, 12
    temperature dependence of, 8, 10

interstellar reddening, 6
IRAF, 20

palindrome sequence, 15
photometric conditions, 15

quantum efficiency, 11
    CCD, 11, 17
    photographic plate, 17
    photomultiplier, 11, 17
    solid state detector, 17

skynoise, 21
star clusters, reasons for using, 13
stellar spectra
    temperature dependence of, 2
stellar temperature
    determination of, 2, 4
    importance of, 2

West Mountain Observatory, 15, 16

zeropoint corrections, 22